SUPPORTING INFORMATION

Supplementary Text

Appendix 1. Field sampling and tree-ring measurements

Data from 20 sites ranging from Mediterranean to Boreal latitudes were sampled, measured and analysed within the scope of the European Union funded project ISONET (EVK2-2001-00237). The network design was based on a number of key criteria including stand age and spatial distribution across Europe, and species are limited to the *Pinus* and *Quercus* genera (plus one *Cedrus atlantica* site in Morocco). These criteria resulted in the preferential selection of sites from non-treeline locations (~75% of the sites), which are more representative of European forests than typical dendrochronological datasets. Three sites were discarded from the original network (total of 23 sites) because they were located over 1,000 km apart from the nearest site (one site in southern Italy) or because they could not be properly assigned to a climate type consistent with that of nearby sites (two sites from high-elevation forests of the Alps) (see the main text for details). Mean annual temperature varied between –1.2°C and 11.5°C among sites, with January being the coldest month (range –14.1 to 5.1°C) and July being the warmest month (11.9 to 19.6°C). Mean annual precipitation was highly variable, ranging from 432 mm to 1,517 mm across sites (Climatic Research Unit, CRU TS 3.21; Harris et al., 2014). Water deficit (i.e., evapotranspiration exceeding precipitation) occured for periods of up to seven months (from March to October) depending on the geographic location, with summer drought (June to August) being a common feature at most sites (Table 1 of main text).

Increment cores were extracted from numerous dominant trees at each site (mean = 46; median = 28) (Table S1), and tree-ring width (TRW) series were produced and cross-dated following standard dendrochronological procedures (Cook & Kairiukstis, 1990). TRW was measured under a binocular microscope with precision of 0.01 mm. Visual cross-dating and ring-width measurements were validated using the program COFECHA (Holmes, 1983). Individual series were then subjected to detrending with the Friedman supersmoother spline (Friedman, 1984) and posterior autoregressive modelling to remove serial autocorrelation. This procedure aims at eliminating biological growth trends and potential disturbance effects and generates stationary (mean = 1) series of dimensionless residual indices (TRW_i) that preserve a common variance at interannual time scales (i.e., high-frequency variability potentially related to climate). Finally, site chronologies were obtained by averaging the indexed values of the

series using a bi-weight robust mean (Cook & Kairiukstis, 1990). These procedures were performed using the program ARSTAN (Cook & Krusic, 2013). The quality of the resulting site chronologies was evaluated by calculation of the mean inter-series correlation (*Rbar*) and the Expressed Population Signal (*EPS*) statistics. An *EPS* value of 0.85 was used to evaluate adequacy of the sample size for capturing a trustworthy population signal (Wigley, Briffa, & Jones, 1984). All chronologies were found to be well replicated during the 20th century (Table S1).

At least two accurately dated intact cores with clear ring boundaries and absence of missing rings from four or more trees per site were selected for subsequent carbon isotope analyses (Treydte et al., 2007). Annual tree rings were separated under a microscope using a scalpel. In general, the whole ring was analyzed for conifers, whereas only latewood was used for oaks to avoid carry-over effects from previous year reserves on earlywood production (Helle & Schleser, 2004). At most sites, rings corresponding to the same year from different trees were pooled and milled to provide enough material for isotope analysis. To remove extractives and lignin from wood samples, α-cellulose was extracted following standard protocols (Boettger et al., 2007). Carbon was extracted from samples as CO_2 using conventional combustion methods. Isotope ratios were expressed as per mil deviations from international standards using the δ notation (Vienna Pee Dee Belemnite, VPDB). Overall accuracy of the analyses (SD of working standards) was 0.06‰.

To account for changes in $\delta^{13}C$ of atmospheric CO_2 ($\delta^{13}C_{air}$) due to fossil fuel combustion, carbon isotope discrimination ($\Delta^{13}C$) was estimated from $\delta^{13}C_{air}$ and α-cellulose $\delta^{13}C$ in plant material ($\delta^{13}C$), as described by Farquhar et al. (1989):

$$\Delta^{13}C = \frac{\delta^{13}C_{air} - \delta^{13}C}{1 + (\delta^{13}C / 1000)} \quad (1)$$

$\delta^{13}C_{air}$ was inferred from data of Antarctic ice-core records, together with modern data from two Antarctic stations (Halley Bay and Palmer Station) of the CU-INSTAAR/NOAA-CMDL network (Ferrio, Araus, Buxó, Voltas, & Bort, 2005). According to these records, the $\delta^{13}C_{air}$ values varied between −6.64‰ and −8.09‰ for the period 1901–2003.

Indexed carbon isotope discrimination chronologies ($\Delta^{13}C_i$) were obtained following the same procedure as described for ring-width chronologies. Hence, any physiological long-term trend (e.g., decadal-scale variability) such as a potential change in the response of trees to increased atmospheric CO_2 (McCarroll et al., 2009; Treydte et al., 2009) was assumed to be removed from the isotopic time series. In this way, we prioritized to investigate the

physiological basis of tree-ring growth responses to high-frequency (interannual) climate variability.

Appendix 2. Tree-ring chronology characteristics

The ring-width chronologies had mean inter-series correlations (*Rbar)* ranging from 0.25 (*Pinus sylvestris* in Poland) to 0.49 (*Quercus petraea* in Germany) (Table S1). *Rbar* did not differ between hardwoods and conifers (mean = 0.40 *vs.* 0.35, respectively; two-tailed Student *t*-test, $P > 0.05$), indicating similar internal coherence of chronologies in both functional groups. In general, hardwoods showed greater absolute radial growth than conifers (mean = 1.42 mm yr^{-1} *vs.* 0.67 mm yr^{-1}; $P < 0.001$). Temperate forests from central Europe situated at the core of the distribution areas of most species (~ 45°–55°N) also showed greater radial growth than geographically peripheral populations (mean = 1.18 mm yr^{-1} *vs.* 0.65 mm yr^{-1}; $P < 0.05$) (Table S1). Growth fluctuations were similar in both inner and outer populations (mean coefficient of variation, $\overline{CV}$ = 26.4% *vs*. 24.0%; $P > 0.05$). The distribution of mean ring-width values across the network was not related to latitude nor longitude; however, there was a significantly negative altitudinal gradient in radial growth ($r = –0.55$, $P < 0.05$). Site mean radial growth was also positively related to mean annual temperature [MAT] ($r = 0.50$, $P < 0.05$) and negatively related to potential evapotranspiration [PET] ($r = 0.53$, $P < 0.05$).

At the site level, eleven chronologies showed a positive basal are increment (BAI) trend and one chronology a negative BAI trend over time (slope *b*, $P < 0.05$) for the period 1901–2003, while no significant trend was detected for the remaining seven chronologies (Table S1). Growth acceleration mainly corresponded to hardwoods (eight sites). Besides, a slight growth enhancement was observed in conifers at cold-limited sites (e.g., Fennoscandia), while significant growth decline was found in a Mediterranean site.

Hardwoods consistently showed higher $\Delta^{13}C$ values than conifers (mean = 18.6‰ *vs.* 17.0‰, respectively; $P < 0.01$), while $\Delta^{13}C$ fluctuations were not statistically different ($\overline{CV}$ = 3.9% *vs*. 3.4%; $P > 0.05$). When considering hardwoods and conifers together, there were significant positive relationship between site mean $\Delta^{13}C$ and latitude ($r = 0.46$, $P < 0.05$) and a negative relationship between site mean $\Delta^{13}C$ and elevation ($r = –0.69$, $P < 0.01$). The observed spatial patterns of $\Delta^{13}C$ were primarily driven by conifers, which covered a larger geographical area as compared to hardwoods (Table 1). PET also explained a sizeable fraction of variation in $\Delta^{13}C$ for conifers ($r = –0.71$, $P < 0.05$), whereas MAT and mean annual precipitation [MAP]

were unrelated to site mean isotope values. The relationship between site mean $\Delta^{13}C$ and ring-width was significant across Europe ($r = 0.60$, $P < 0.01$)

Appendix 3. Random modelling analysis

3.1. Temporal coherence of ring-width signals among chronologies

The investigation of common ring-width fluctuations among chronologies (i.e., common signal strength) was performed through mixed modelling as described in Shestakova et al. (2014). Let W_{ij} stand for TRW_i of the *i*th chronology in the *j*th year. Then the estimators can be defined in terms of the following random model:

$$W_{ij} = Y_j + e_{ij} \quad (2)$$

where Y_j is a random effect of the *j*th year and e_{ij} is a random deviation of the *i*th chronology in the *j*th year. Here, we assume that the year effects behave as if they came from a normal distribution with mean zero and variance σ_Y^2. We also assume that random effects from different random terms (Y_j and e_{ij}) are independent of each other (Demidenko, 2004). The reproducibility of observations by the set of *I* chronologies (i = 1 to n) can be estimated as (Shestakova et al., 2014):

$$\hat{a} = \frac{\sigma_Y^2}{\sigma_Y^2 + \sigma_e^2} \quad (3)$$

We refer to $\hat{a}$ as the intra-class correlation or growth synchrony among chronologies. Intra-class correlation close to 1 indicates near-perfect synchrony among chronologies, while a value close to 0 denotes spatial asynchrony.

If we hypothesize about the presence of different sources of similarities–dissimilarities among tree-ring records (e.g., pertinence to a particular climate type), then model (2) can be expanded to an alternative mixed model by adding a fixed effect β_r (r = 1 to m). In this case, the estimators can be defined as follows:

$$W_{ijr} = \beta_r + Y_{jr} + e_{ijr} \quad (4)$$

where β_r is a fixed term accounting for mean differences among the m groups, Y_{jr} is the random effect of the j^{th} year in the r^{th} group, and e_{ijr} is the residual term (i.e., a random deviation of the i^{th} chronology in the j^{th} year within the r^{th} group).

To analyse temporal patterns in synchrony within and between groups with distinct growth signals, corresponding to the five climate types (r = 1 to 5; see Materials and Methods

section for details), the following variance-covariance (VCOV) structure underlying model was employed (Shestakova et al., 2014):

$\mathrm{cov}(\underline{Y}_{jr};\underline{Y}_{jr^*}) = \sigma^2_{Y_r}$, when $r = r^*$,

otherwise $\mathrm{cov}(\underline{Y}_{jr};\underline{Y}_{jr^*}) = \sigma^2_{Y_{rr^*}}$

This structure allows each group to have its own year variance and each pair of groups its own year covariance. The mean correlation (synchrony) estimated between all possible of chronologies as in Eq. 2 can be split into (i) a mean correlation between pairs of within every group *r* and (ii) a mean correlation between pairs of chronologies belonging to groups r and r^*, as follows (Shestakova et al., 2014):

$$\hat{a}_{Cw} = \frac{\sigma^2_{Y_r}}{\sigma^2_{Y_r} + \sigma^2_e} \quad (5)$$

$$\hat{a}_{Cb} = \frac{\sigma^2_{Y_{rr^*}}}{\sqrt{(\sigma^2_{Y_r} + \sigma^2_e) \times (\sigma^2_{Y_{r^*}} + \sigma^2_e)}} \quad (6)$$

Mixed models allow for flexible modelling of complex intra- and inter-group correlation patterns and heteroscedastic errors, hence providing estimates to solve Eqs. (5) (6). Variance–covariance (VCOV) structures used to model tree-ring signals in this study are provided in Table S2.

3.2. Relationships between radial growth and stable isotopes

The temporal associations between traits (TRW_i, $\Delta^{13}C_i$) were investigated at the group level through bivariate analyses (Holland, 2006). Following Shestakova et al. (2017), the single random model (2) was extended to take into account simultaneously the information available on a pair of traits (TRW_i and $\Delta^{13}C_i$) as follows: the temporal (yearly) component of a Pearson correlation between traits (which also includes residual cross-product effects) was estimated partitioning the general covariance (i.e., across years and chronologies) into its year and residual components. In particular, the correlation of year effects (r_Y) was calculated as:

$$r_Y = \frac{\sigma_{Y_{12}}}{\sqrt{\sigma^2_{Y_1} \times \sigma^2_{Y_2}}} \quad (7)$$

where $\sigma_{Y_{12}}$ is the common variability (covariance) of year effects underlying traits 1 and 2, $\sigma^2_{Y_1}$ stands for the variance of year effects for trait 1 and $\sigma^2_{Y_2}$ stands for the variance of year effects for trait 2.

The statistical analyses were performed with SAS/STAT (ver. 9.4, SAS Inc., Cary, NC, USA). We used the MIXED procedure for variance-covariance modelling and estimation of variance components through restricted maximum likelihood (REML). Specifically, combined variance-covariance estimation of two traits by multivariate REML analysis was implemented through the RANDOM statement using a full (or unstructured) variance-covariance matrix (Holland, 2006).

Appendix 4. Additional evaluation of geographical trends in growth synchrony

To guarantee the scope of our inferences in growth synchrony across Europe, we examined an independent, larger dataset of ring-width chronologies available from the International Tree-Ring Data Bank (ITRDB) (Grissino-Mayer & Fritts, 1997). The criteria for inclusion in the dataset were as follows: (*i*) geographic coverage = European continent; (*ii*) time span = 1901–1998 or larger (i.e., common time period for ISONET chronologies); and (*iii*) taxonomy = membership to the same species used in the ISONET network. In total, 103 site chronologies met these requirements. For these chronologies, we checked for spatial distribution across the continent, selecting those that could be classified into potential groups having a sufficient amount of chronologies ($n \geq 4$) (given the pre-requisite of 1,000 km as maximum distance between sites). Indexed ring-width chronologies were built for each site following the same procedure as described in Materials and Methods. As a result, 80 chronologies were assigned to eight groups (Fig. S5a), which were used for subsequent estimation of growth synchrony ($\hat{a}$) and assessment of geographical patterns in $\hat{a}$. In this case, latitude was positively related to longitude ($r = 0.91$, $P < 0.01$) but there were not associations between elevation and either latitude or longitude.

Supplementary References

Boettger, T., Haupt, M., Knöller, K., Weise, S. M., Waterhouse, J. S., Rinne, K. T., Loader, N. J., Sonninen, E., Jungner, H., Masson-Delmotte, V., Stievenard, M., Guillemin, M.-T., Pierre, M., Pazdur, A., Leuenberger, M., Filot, M., Saurer, M., Reynolds, C. E., Helle, G., & Schleser, G. H. (2007). Wood cellulose preparation methods and mass spectrometric analyses of $\delta^{13}C$, $\delta^{18}O$, and nonexchangeable $\delta^{2}H$ values in cellulose, sugar, and starch: an interlaboratory comparison. *Analytical Chemistry*, **79**, 4603–4612.

Cook, E. R., & Kairiukstis, L. A. (1990). *Methods of dendrochronology: Applications in the environmental sciences*. Dordrecht, Netherlands: Springer Netherlands.

Cook, E. R., & Krusic, P. J. (2013). *Program ARSTAN. A tree-ring standardization program based on detrending and autoregressive time series modeling, with interactive graphics*. Palisades, NY: Columbia University.

Demidenko, E. (2004). *Mixed models: theory and applications*. New York, NY: John Wiley & Sons.

Ferrio, J. P., Araus, J. L., Buxó, R., Voltas, J., & Bort, J. (2005). Water management practices and climate in ancient agriculture: inferences from the stable isotope composition of archaeobotanical remains. *Vegetation History and Archaeobotany*, **14**, 510–517.

Friedman, J. H. (1984). *A variable span smoother*. Stanford, CA: Stanford University.

Grissino-Mayer, H. D., & Fritts, H. C. (1997). The International Tree-Ring Data Bank: an enhanced global database serving the global scientific community. *Holocene*, **7**, 235–228.

Helle, G., & Schleser, G. H. (2004). Beyond CO_2-fixation by Rubisco – an interpretation of $^{13}C/^{12}C$ variations in tree rings from novel intra-seasonal studies on broad-leaf trees. *Plant, Cell and Environment*, **27**, 367–380.

Holland, J. B. (2006). Estimating genotypic correlations and their standard errors using multivariate restricted maximum likelihood estimation with SAS Proc MIXED. *Crop Science*, **46**, 642–654.

Holmes, R. L. (1983). Computer-assisted quality control in tree-ring dating and measurement. *Tree Ring Bulletin*, **43**, 69–78.

McCarroll, D., Gagen, M. H., Loader, N. J., Robertson, I., Anchukaitis, K. J., Los, S., Young, G. H. F, Jalkanen, R., Kirchhefer, A., & Waterhouse, J. S. (2009). Correction of tree ring stable carbon isotope chronologies for changes in the carbon dioxide content of the atmosphere. *Geochimica et Cosmochimica Acta*, **73**, 1539–1547.

Treydte, K., Frank, D. C., Esper, J., Andreu, L., Bednarz, Z., Berninger, F., Boettger, T., D'Alessandro, C. M., Etien, N., Filot, M., Grabner, M., Guillemin, M. T., Gutierrez, E., Haupt, M., Helle, G., Hilasvuori, E., Jungner, H., Kalela-Brundin, M., Krapiec, M., Leuenberger, M., Loader, N. J., Masson-Delmotte, V., Pazdur, A., Pawelczyk, S., Pierre, M., Planells, O., Pukiene, R., Reynolds-Henne, C. E., Rinne, K. T., Saracino, A., Saurer, M., Sonninen, E., Stievenard, M., Switsur, V. R., Szczepanek, M., Szychowska-Krapiec, E., Todaro, L., Waterhouse, J. S., Weigl, M., & Schleser, G. H. (2007). Signal strength and climate calibration of a European tree-ring isotope network. *Geophysical Research Letters*, **34**, L24302.

Treydte, K., Frank, D. C., Saurer, M., Helle, G., Schleser, G. H., & Esper, J. (2009). Impact of climate and CO_2 on a millennium-long tree-ring carbon isotope record. *Geochimica et Cosmochimica Acta*, **73**, 4635–4647.

Wigley, T. M. L., Briffa, K. R., & Jones, P. D. (1984). On the average value of correlated time series, with applications in dendroclimatology and hydrometerology. *Journal of Applied Meteorology and Climatology*, **23**, 201–213.

Supplementary Tables

Table S1. Dendrochronological characteristics of the sampling sites. Mean values are calculated over the period 1901–2003. Abbreviations: *EPS*, Expressed Population Signal; *Rbar*, mean interseries correlation; TRW, tree-ring width; $\Delta^{13}C$, carbon isotope discrimination. The variability of mean values is expressed as standard deviation (SD).

No	Code	Species	No. trees/cores	Time span	*EPS* > 0.85 since	*Rbar*±SD	TRW±SD (mm)	$\Delta^{13}C$±SD (‰)
1	Ina	*Pinus sylvestris*	15/32	1508–2003	1570	0.44±0.10	0.52±0.15	18.46±0.44
2	Ilo	*Pinus sylvestris*	28/39	1580–2003	1610	0.33±0.07	0.29±0.04	17.81±0.40
3	Gut	*Pinus sylvestris*	45/89	1449–2004	1510	0.45±0.10	0.50±0.08	17.39±0.54
4	Bro	*Quercus robur*	7/19	1822–2004	1850	0.44±0.13	1.84±0.60	18.90±0.74
5	Loc	*Quercus robur*	28/38	1706–2003	1750	0.29±0.14	1.16±0.25	19.30±0.58
6	Pan	*Pinus sylvestris*	30/61	1487–2003	1590	0.28±0.11	0.79±0.21	16.93±0.54
7	Suw	*Pinus sylvestris*	76/76	1600–2004	1620	0.31±0.14	1.02±0.28	17.10±0.80
8	Wob	*Quercus robur*	20/30	1613–2003	1640	0.44±0.11	1.37±0.24	17.37±0.91
9	Dra	*Quercus petraea*	16/45	1770–2002	1800	0.49±0.11	1.42±0.49	17.53±0.68
10	Win	*Pinus sylvestris*	16/21	1763–2003	1790	0.28±0.12	1.22±0.31	16.90±0.62
11	Nie1	*Quercus robur*	35/39	1768–2003	1810	0.37±0.11	1.88±0.40	19.83±0.91
12	Nie2	*Pinus sylvestris*	72/78	1622–2003	1650	0.25±0.15	1.01±0.32	17.36±0.98
13	Fon	*Quercus petraea*	30/60	1306–2000	1530	0.31±0.13	0.87±0.31	17.85±0.72
14	Ren	*Quercus robur*	11/30	1751–1998	1860	0.43±0.17	1.63±0.53	18.89±0.45
15	Lai	*Quercus petraea*	55/81	1462–2003	1510	0.39±0.17	1.18±0.18	18.86±0.71
16	Poe	*Pinus nigra*	326/588	1319–2002	1500	0.37±0.11	0.62±0.18	18.32±0.60
17	Lil	*Pinus sylvestris*	15/32	1511–2002	1560	0.35±0.10	0.47±0.12	16.22±0.55
18	Ped	*Pinus uncinata*	23/56	1269–2003	1510	0.33±0.09	0.49±0.10	15.91±0.51
19	Caz	*Pinus nigra*	33/68	1125–2002	1190	0.47±0.10	0.47±0.09	15.03±0.41
20	Col	*Cedrus atlantica*	10/40	1560–2000	1590	0.51±0.09	1.12±0.26	14.50±0.42

Table S2. Description of variance-covariance (VCOV) models accommodating between- and within-group variability (adapted from Shestakova al. [2014] and Shestakova et al. [2018]). The models constrain different elements of the year × group (G) variance-covariance structure. The residual (R) variance-covariance structure is a diagonal matrix with constant (homogeneous residuals, HR) or non-constant (heterogeneous residuals, HeR) terms. The number of parameters to be estimated is shown for each model (#par).

Hypothesis testing	G matrix	R matrix – HR	R matrix – HeR	#par (HR / HeR)
Broad evaluation. Null model ignoring groups	σ^2	σ_ε^2	–	2 / –
Narrow evaluation. Lack of common signal between groups	$\begin{pmatrix} \sigma_1^2 & 0 & 0 & 0 & 0 \\ 0 & \sigma_2^2 & 0 & 0 & 0 \\ 0 & 0 & \sigma_3^2 & 0 & 0 \\ 0 & 0 & 0 & \sigma_4^2 & 0 \\ 0 & 0 & 0 & 0 & \sigma_5^2 \end{pmatrix}$	σ_ε^2	$\begin{pmatrix} \sigma_{\varepsilon_1}^2 & 0 & 0 & 0 & 0 \\ 0 & \sigma_{\varepsilon_2}^2 & 0 & 0 & 0 \\ 0 & 0 & \sigma_{\varepsilon_3}^2 & 0 & 0 \\ 0 & 0 & 0 & \sigma_{\varepsilon_4}^2 & 0 \\ 0 & 0 & 0 & 0 & \sigma_{\varepsilon_5}^2 \end{pmatrix}$	6 / 20
Compound symmetry. Constant variance and covariance	$\begin{pmatrix} \sigma^2+\sigma_1 & \sigma_1 & \sigma_1 & \sigma_1 & \sigma_1 \\ \sigma_1 & \sigma^2+\sigma_1 & \sigma_1 & \sigma_1 & \sigma_1 \\ \sigma_1 & \sigma_1 & \sigma^2+\sigma_1 & \sigma_1 & \sigma_1 \\ \sigma_1 & \sigma_1 & \sigma_1 & \sigma^2+\sigma_1 & \sigma_1 \\ \sigma_1 & \sigma_1 & \sigma_1 & \sigma_1 & \sigma^2+\sigma_1 \end{pmatrix}$	σ_ε^2	$\begin{pmatrix} \sigma_{\varepsilon_1}^2 & 0 & 0 & 0 & 0 \\ 0 & \sigma_{\varepsilon_2}^2 & 0 & 0 & 0 \\ 0 & 0 & \sigma_{\varepsilon_3}^2 & 0 & 0 \\ 0 & 0 & 0 & \sigma_{\varepsilon_4}^2 & 0 \\ 0 & 0 & 0 & 0 & \sigma_{\varepsilon_5}^2 \end{pmatrix}$	3 / 7
Heterogeneous Toeplitz. Different variances and covariances for all group pairs depending on their geographic proximity	$\begin{pmatrix} \sigma_1^2 & \sigma_1\sigma_2\rho_1 & \sigma_1\sigma_3\rho_2 & \sigma_1\sigma_4\rho_3 & \sigma_1\sigma_5\rho_4 \\ \sigma_1\sigma_2\rho_1 & \sigma_2^2 & \sigma_2\sigma_3\rho_1 & \sigma_2\sigma_4\rho_2 & \sigma_2\sigma_5\rho_3 \\ \sigma_1\sigma_3\rho_2 & \sigma_2\sigma_3\rho_1 & \sigma_3^2 & \sigma_3\sigma_4\rho_1 & \sigma_3\sigma_5\rho_2 \\ \sigma_1\sigma_4\rho_3 & \sigma_2\sigma_4\rho_2 & \sigma_3\sigma_4\rho_1 & \sigma_4^2 & \sigma_4\sigma_5\rho_1 \\ \sigma_1\sigma_5\rho_4 & \sigma_2\sigma_5\rho_3 & \sigma_3\sigma_5\rho_2 & \sigma_4\sigma_5\rho_1 & \sigma_5^2 \end{pmatrix}$	σ_ε^2	$\begin{pmatrix} \sigma_{\varepsilon_1}^2 & 0 & 0 & 0 & 0 \\ 0 & \sigma_{\varepsilon_2}^2 & 0 & 0 & 0 \\ 0 & 0 & \sigma_{\varepsilon_3}^2 & 0 & 0 \\ 0 & 0 & 0 & \sigma_{\varepsilon_4}^2 & 0 \\ 0 & 0 & 0 & 0 & \sigma_{\varepsilon_5}^2 \end{pmatrix}$	10 / 14

Heterog. Toeplitz with two bands. Different variances and (co)variances for contiguous group pairs only	$\begin{pmatrix} \sigma_1^2 & \sigma_1\sigma_2\rho_1 & 0 & 0 & 0 \\ \sigma_1\sigma_2\rho_1 & \sigma_2^2 & \sigma_2\sigma_3\rho_1 & 0 & 0 \\ 0 & \sigma_2\sigma_3\rho_1 & \sigma_3^2 & \sigma_3\sigma_4\rho_1 & 0 \\ 0 & 0 & \sigma_3\sigma_4\rho_1 & \sigma_4^2 & \sigma_4\sigma_5\rho_1 \\ 0 & 0 & 0 & \sigma_4\sigma_5\rho_1 & \sigma_5^2 \end{pmatrix}$	σ_ε^2	$\begin{pmatrix} \sigma_{\varepsilon_1}^2 & 0 & 0 & 0 & 0 \\ 0 & \sigma_{\varepsilon_2}^2 & 0 & 0 & 0 \\ 0 & 0 & \sigma_{\varepsilon_3}^2 & 0 & 0 \\ 0 & 0 & 0 & \sigma_{\varepsilon_4}^2 & 0 \\ 0 & 0 & 0 & 0 & \sigma_{\varepsilon_5}^2 \end{pmatrix}$	7 / 11
Heterog. Toeplitz with three bands. Different variances and (co)variances for contiguous group pairs of first and second order.	$\begin{pmatrix} \sigma_1^2 & \sigma_1\sigma_2\rho_1 & \sigma_1\sigma_3\rho_2 & 0 & 0 \\ \sigma_1\sigma_2\rho_1 & \sigma_2^2 & \sigma_2\sigma_3\rho_1 & \sigma_2\sigma_4\rho_2 & 0 \\ \sigma_1\sigma_3\rho_2 & \sigma_2\sigma_3\rho_1 & \sigma_3^2 & \sigma_3\sigma_4\rho_1 & \sigma_3\sigma_5\rho_2 \\ 0 & \sigma_2\sigma_4\rho_2 & \sigma_3\sigma_4\rho_1 & \sigma_4^2 & \sigma_4\sigma_5\rho_1 \\ 0 & 0 & \sigma_3\sigma_5\rho_2 & \sigma_4\sigma_5\rho_1 & \sigma_5^2 \end{pmatrix}$	σ_ε^2	$\begin{pmatrix} \sigma_{\varepsilon_1}^2 & 0 & 0 & 0 & 0 \\ 0 & \sigma_{\varepsilon_2}^2 & 0 & 0 & 0 \\ 0 & 0 & \sigma_{\varepsilon_3}^2 & 0 & 0 \\ 0 & 0 & 0 & \sigma_{\varepsilon_4}^2 & 0 \\ 0 & 0 & 0 & 0 & \sigma_{\varepsilon_5}^2 \end{pmatrix}$	8 / 12
Unstructured. Completely general covariance matrix	$\begin{pmatrix} \sigma_1^2 & \sigma_{12} & \sigma_{13} & \sigma_{14} & \sigma_{15} \\ \sigma_{12} & \sigma_2^2 & \sigma_{23} & \sigma_{24} & \sigma_{25} \\ \sigma_{13} & \sigma_{23} & \sigma_3^2 & \sigma_{34} & \sigma_{35} \\ \sigma_{14} & \sigma_{24} & \sigma_{34} & \sigma_4^2 & \sigma_{45} \\ \sigma_{15} & \sigma_{25} & \sigma_{35} & \sigma_{45} & \sigma_5^2 \end{pmatrix}$	σ_ε^2	$\begin{pmatrix} \sigma_{\varepsilon_1}^2 & 0 & 0 & 0 & 0 \\ 0 & \sigma_{\varepsilon_2}^2 & 0 & 0 & 0 \\ 0 & 0 & \sigma_{\varepsilon_3}^2 & 0 & 0 \\ 0 & 0 & 0 & \sigma_{\varepsilon_4}^2 & 0 \\ 0 & 0 & 0 & 0 & \sigma_{\varepsilon_5}^2 \end{pmatrix}$	16 / 20

References

Shestakova, T. A., Aguilera, M., Ferrio, J. P., Gutiérrez, E., & Voltas, J. (2014). Unravelling spatiotemporal tree-ring signals in Mediterranean oaks: a variance–covariance modelling approach of carbon and oxygen isotope ratios. *Tree Physiology*, **34**, 819–838.

Shestakova, T. A., Gutiérrez, E., & Voltas, J. (2018). A roadmap to disentangling ecogeographical patterns of spatial synchrony in dendrosciences. *Trees*, **32**, 359–370.

Table S3. Results of variance-covariance models for synchrony analysis. The table lists Akaike and Bayesian information criteria (AIC / BIC). The selected variance-covariance (VCOV) structure for modelling synchrony patterns for the study period (1901–2003) and for each 50-yr moving interval are in bold.

Period	*Broad evaluation*	*Narrow evaluation*	*Compound symmetry*	*Heterogeneous Toeplitz*	*Heterog. Toeplitz with two bands*	*Heterog. Toeplitz with three bands*	*Unstructured*
Study period							
1901–2003	–1714.9 / –1709.6	–1773.9 / –1747.4	–1776.8 / –1758.3	–1781.2 / –1744.2	**–1785.9 / –1756.8**	–1785.0 / –1753.3	–1782.4 / –1729.5
Moving intervals							
1901–1949	–775.7 / –771.9	–814.7 / –797.5	–803.5 / –790.1	–817.1 / –794.1	**–816.7 / –795.6**	–817.8 / –796.8	–817.0 / –780.7
1905–1954	–804.9 / –801.0	–836.4 / –819.2	–827.2 / –813.8	–802.7 / –775.9	**–837.3 / –816.3**	–835.5 / –812.6	–833.6 / –797.3
1910–1959	–765.9 / –762.1	–797.5 / –778.4	–793.6 / –780.2	–804.4 / –777.6	**–806.1 / –785.1**	–805.2 / –782.3	–808.7 / –770.4
1915–1964	–776.0 / –772.2	–796.3 / –779.1	–793.4 / –780.0	–802.7 / –775.9	**–806.6 / –785.6**	–805.3 / –782.4	–813.4 / –777.1
1920–1969	–776.7 / –772.9	–796.2 / –777.1	–796.3 / –783.0	–805.7 / –778.9	**–809.1 / –788.1**	–808.1 / –785.1	–813.6 / –775.3
1925–1974	–798.6 / –794.8	–828.7 / –809.6	–828.2 / –814.8	–836.5 / –809.7	**–839.1 / –818.0**	–838.0 / –815.1	–839.2 / –801.0
1930–1979	–815.2 / –811.3	–851.0 / –831.9	–854.1 / –840.7	–853.9 / –827.2	**–858.0 / –836.9**	–856.0 / –833.0	–849.9 / –811.6
1935–1984	–827.5 / –823.7	–859.9 / –840.8	–864.8 / –851.4	–865.6 / –838.8	**–869.6 / –848.6**	–868.9 / –845.9	–863.1 / –824.9
1940–1989	–794.6 / –790.8	–830.8 / –811.7	**–835.8 / –822.4**	–834.4 / –807.7	–837.2 / –816.2	–838.1 / –815.2	–829.0 / –790.8
1945–1994	–790.3 / –786.5	–819.8 / –800.7	**–827.8 / –814.5**	–820.0 / –793.2	–823.8 / –802.8	–823.7 / –800.7	–812.1 / –773.8
1950–1999	–784.0 / –780.2	–815.5 / –796.4	**–827.0 / –813.6**	–821.3 / –794.5	–823.0 / –802.0	–825.0 / –802.1	–814.0 / –775.8
1955–2003	–738.7 / –734.9	–760.1 / –741.2	**–774.0 / –760.7**	–765.4 / –738.9	–767.2 / –746.4	–768.4 / –745.7	–757.4 / –719.6

Supplementary Figures

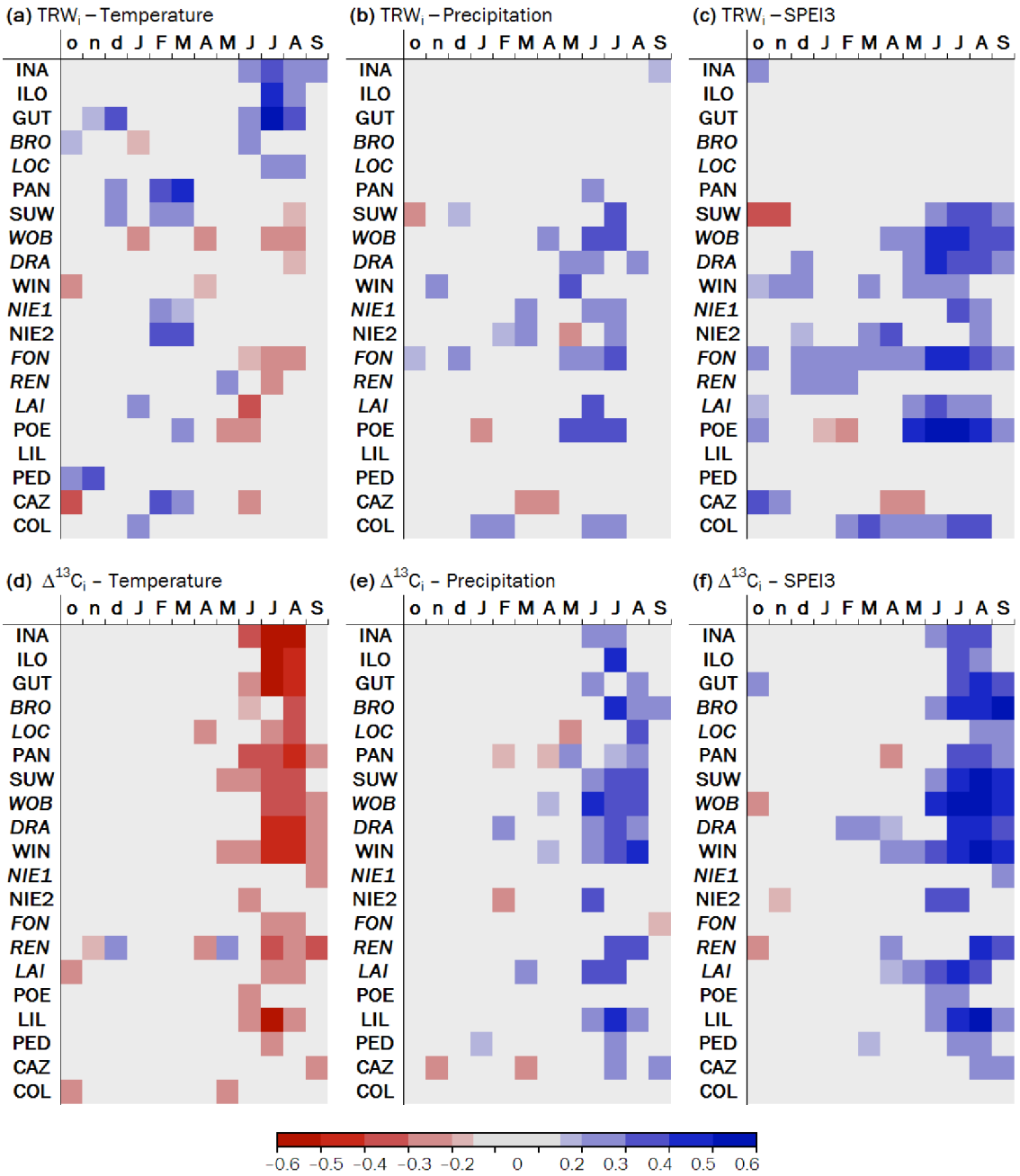

Figure S1. Climate signals at the site level for **(a, b, c)** TRW$_i$, **(d, e, f)** $\Delta^{13}C_i$ for the period 1901–2003. Tree responses to climate are based on bootstrapped correlations between tree-ring chronologies and monthly mean temperature (*left panel*), precipitation (*middle panel*) and 3-month Standardized Precipitation Evapotranspiration Index (SPEI3; *right panel*). Red and blue colors denote negative and positive relationships, respectively. Only significant correlations ($P < 0.05$) are shown. Sites are sorted latitudinally, from north (top) to south (bottom). Lowercase and uppercase letters correspond to months of the years before and during tree-ring formation, respectively.

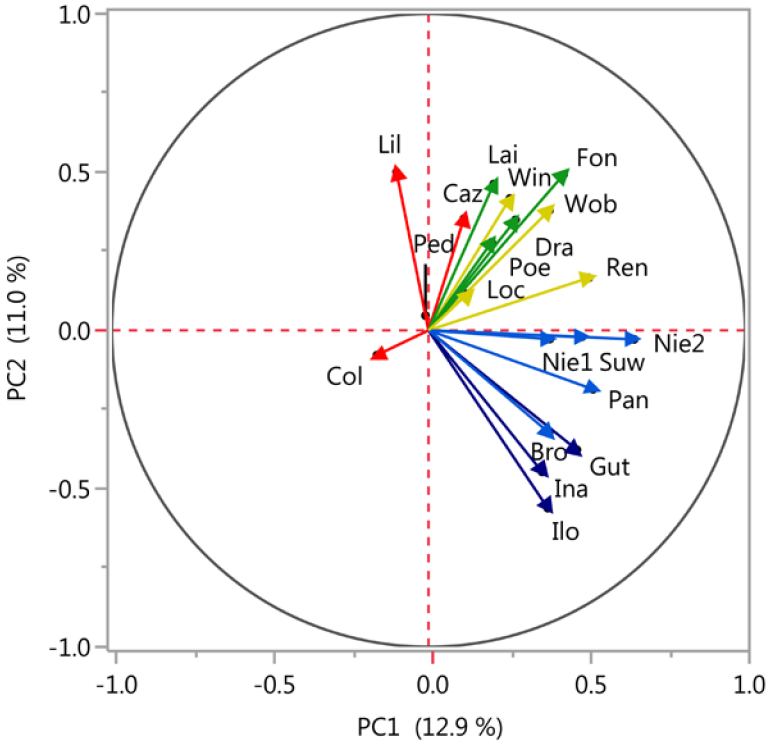

Figure S2. Principal component analysis performed on 19 indexed ring-width chronologies distributed across Europe and northern Africa for the common period 1901–1998. The biplot shows the loadings of the first and second principal components (PC1 and PC2) for each chronology. Colors indicate different groups as in Fig. 2. Codes are as in Table S1.

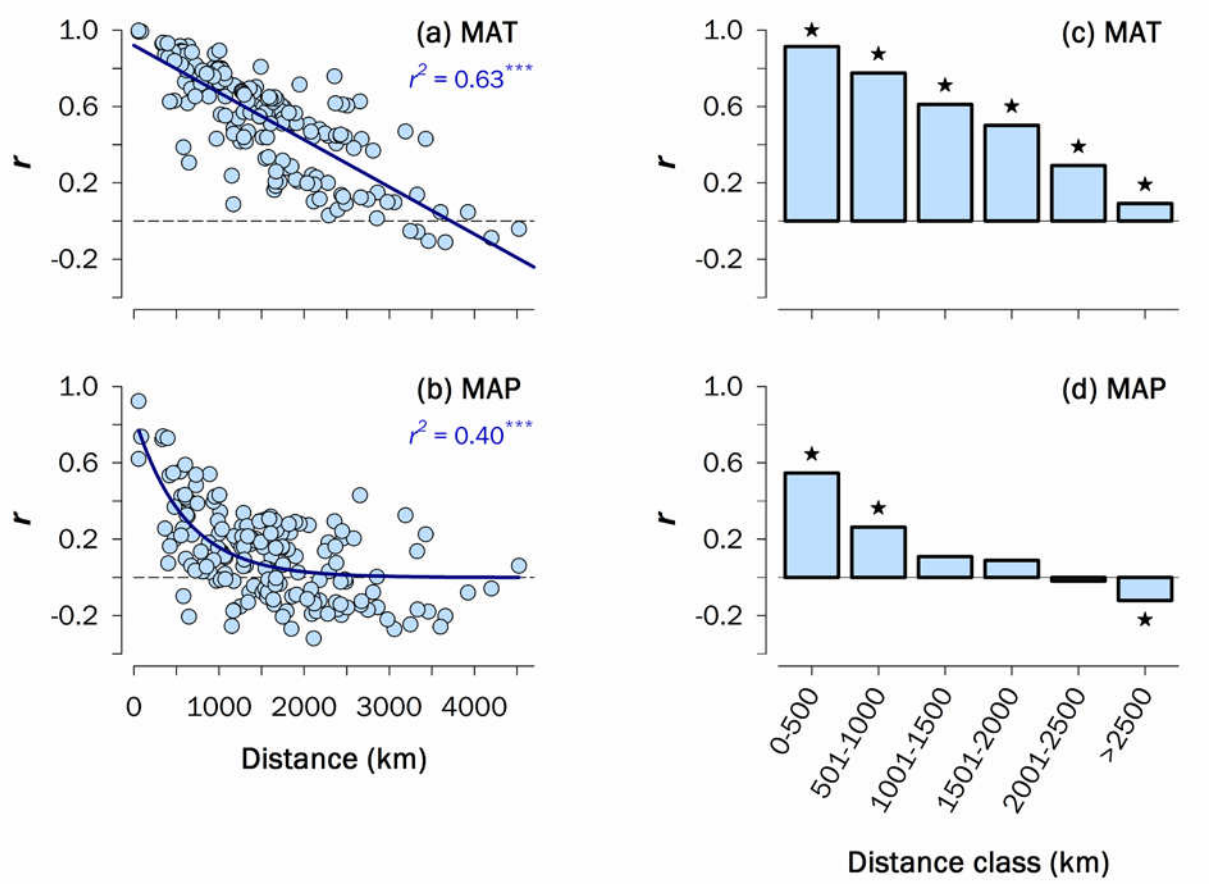

Figure S3.Spatial patterns of climate signals across Europe for the period 1901–2003: **(a, c)** mean annual temperature, MAT, **(b, d)** mean annual precipitation, MAP. Site climate series were obtained from the nearest grid point to each sampling site based on CRU TS 3.21 data. The resulting series were then subjected to linear detrending and autoregressive modelling to remove long-term trends (e.g., global warming) and serial autocorrelation, respectively. *(Left panels)* Pairwise correlations of climate series as a function of geographical distance. The patterns are summarized by regressing the correlation coefficients (r values) involving pairs of temporal series (y-axis) on their corresponding distance (x-axis) by using a linear function for MAT and a negative exponential function ($y = be^{-cx}$) for MAP. Asterisks after the coefficient of determination (r^2) indicate level of significance ($^{***}P < 0.001$). *(Right panels)* Spatial structure of climate patterns across Europe. The spatial autocorrelation in the climate network was characterized for six consecutive distance classes (listed on the x-axis). Mean r values and their statistical significance (P) within each distance class were estimated from 1,000 randomizations. Significant correlation coefficients ($P < 0.05$) are indicated by asterisks.

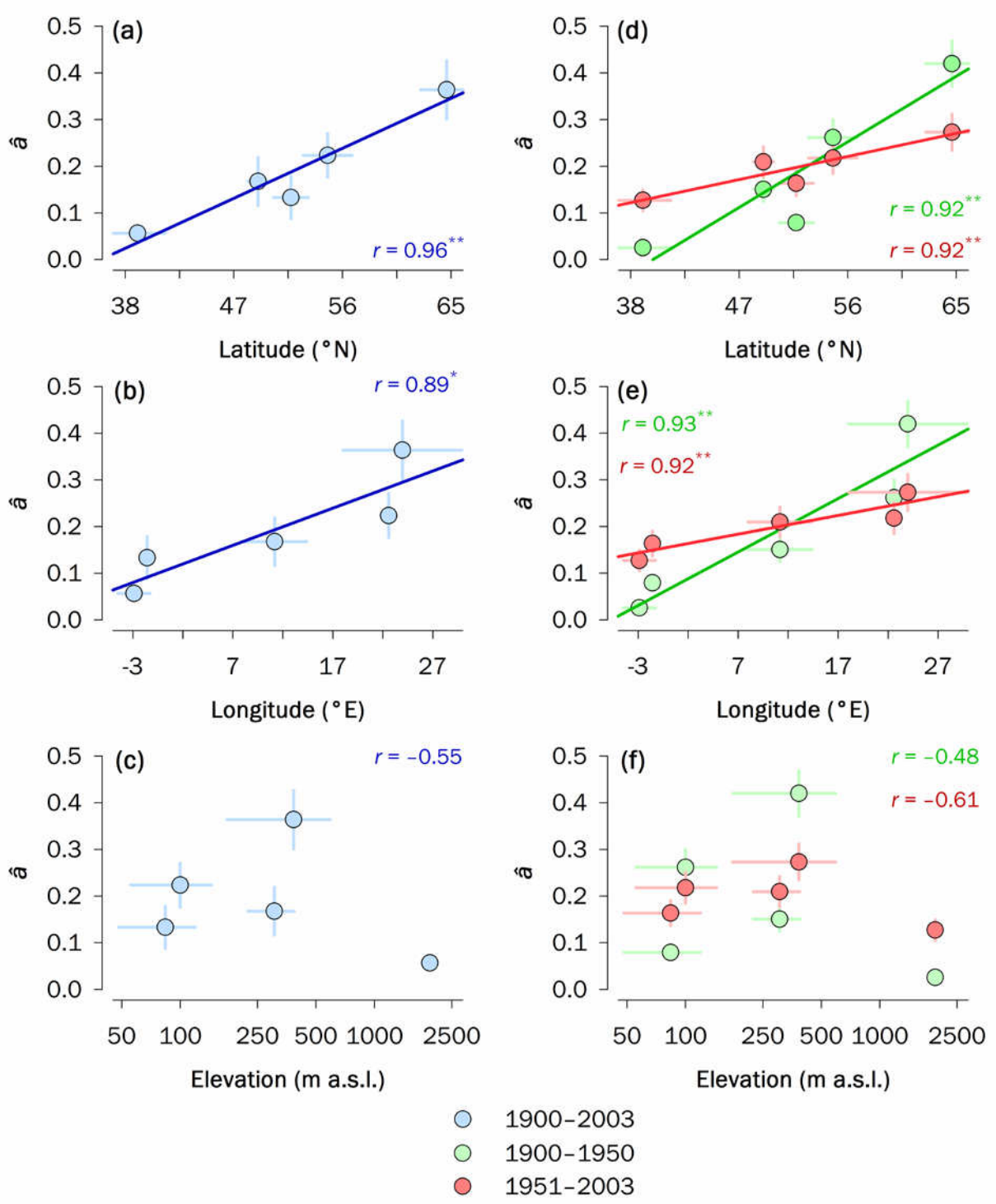

Figure S4. Geographical patterns of growth synchrony ($\hat{a}$) at the group level for the entire period 1901–2003 and change in $\hat{a}$ for two consecutive periods (1901–1950 and 1951–2003).

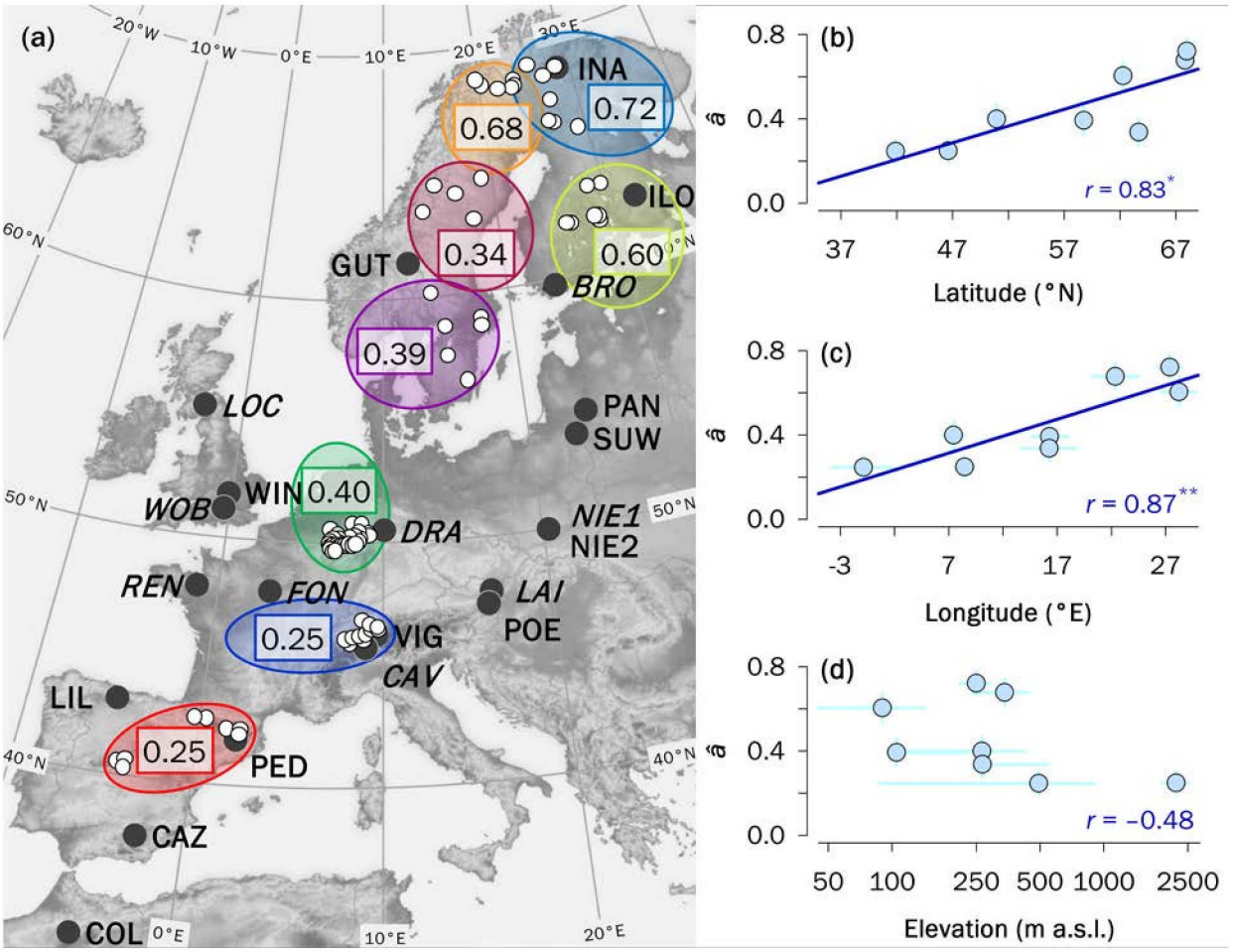

Figure S5. Geographical patterns of growth synchrony ($\hat{a}$) for chronologies obtained from the International Tree-Ring Data Bank (ITRDB) dataset for the period 1901–2003. **(a)** Geographical distribution of sampling sites for two independent datasets: pan-European network ISONET (black dots) and ITRDB (white dots). Colored circles identify groups of neighbouring chronologies obtained from ITRDB ($n = 8$). Numbers indicate $\hat{a}$ values at group level estimated for the period 1901–2003. Spatial patterns of synchrony are characterized as linear regressions of $\hat{a}$ values (y-axis) on their corresponding **(b)** latitude, **(c)** longitude or **(d)** elevation (x-axis). Note that the abscissa in (d) has a logarithmic scale. Significant linear trends along the geographical gradients are depicted as thick lines ($^{*}P < 0.05$; $^{**}P < 0.01$). All calculations are based on indexed ring-width chronologies. Error bars denote standard errors.

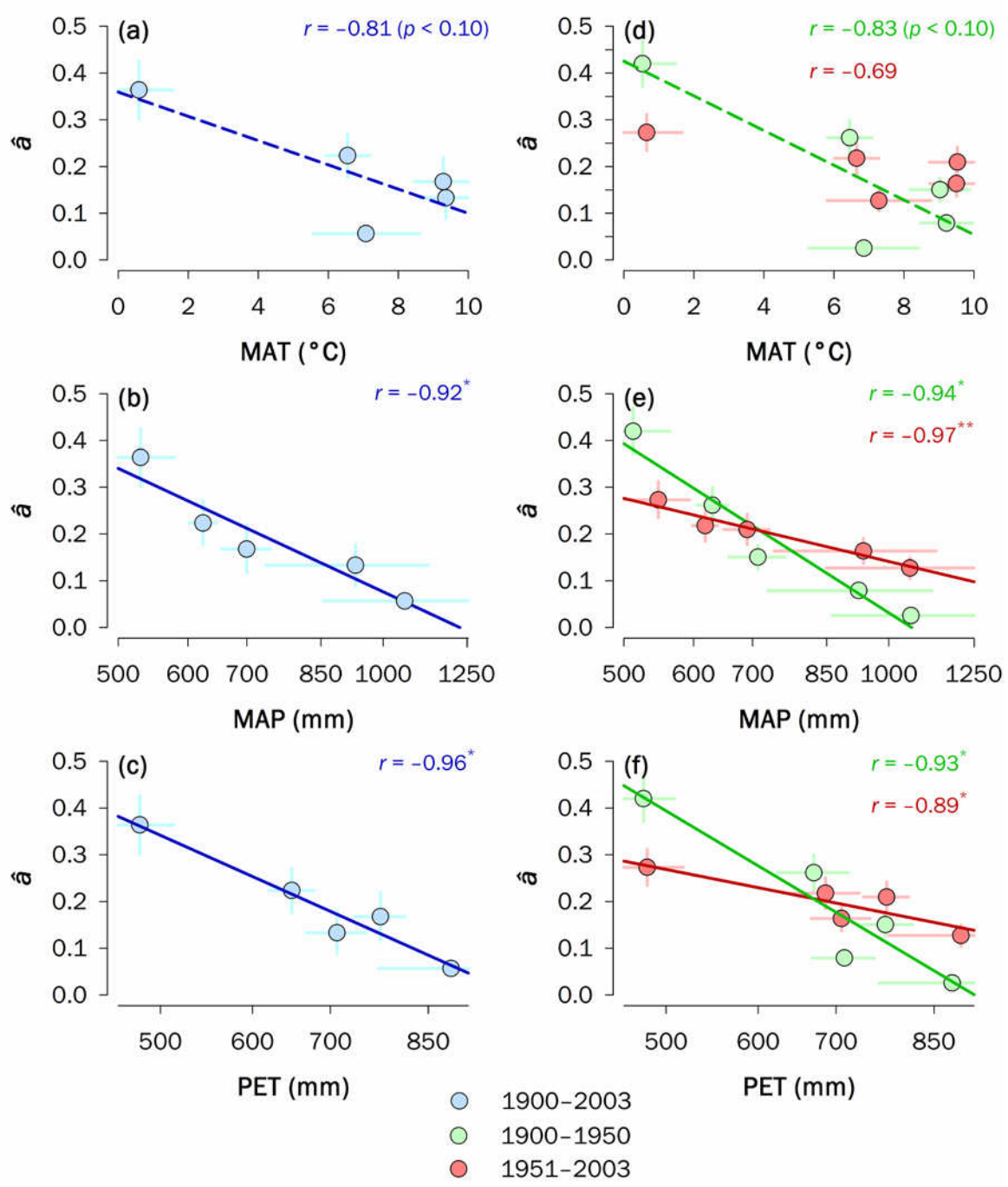

Figure S6. Growth synchrony along climatic gradients. Synchrony patterns ($\hat{a}$) at the group level for the entire period 1901–2003 *(left panels)* and for two consecutive periods (1901–1950 and 1951–2003) (*right panels*) as a function of **(a, d)** mean annual temperature (MAT), **(b, e)** mean annual precipitation (MAP), and (**c, f)** mean annual potential evapotranspiration (PET). The patterns are characterized as linear regressions of growth synchrony for each group (*y*-axis) on its corresponding mean climate variable (*x*-axis). Significant linear trends along the climatic gradients are depicted as thick lines ($^{*}P < 0.05$; $^{**}P < 0.01$; $^{***}P < 0.001$). Error bars denote standard errors.

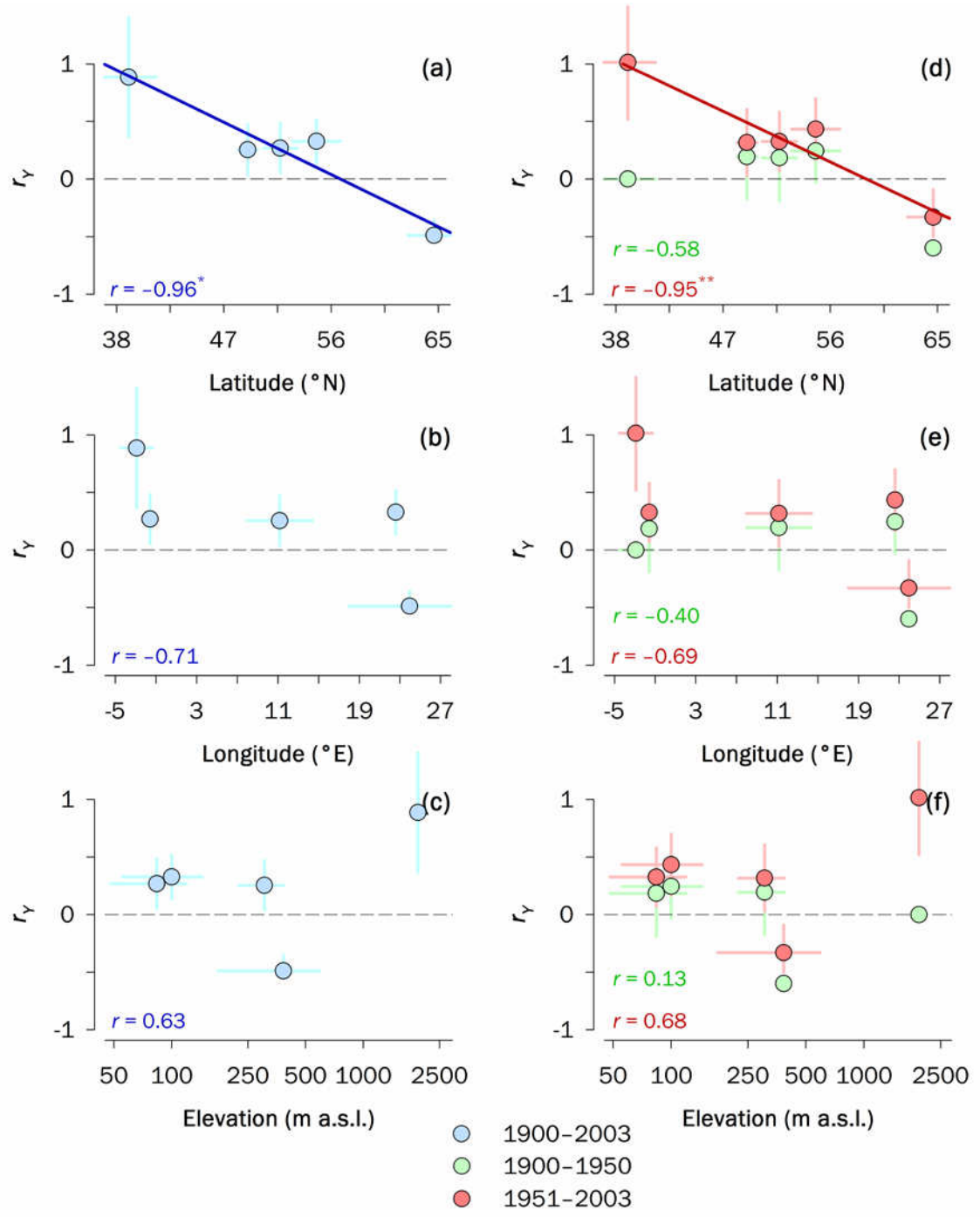

Figure S7. Geographical patterns of the relationship between indexed tree-ring width (TRW_i) and carbon isotope discrimination ($\Delta^{13}C_i$) chronologies across Europe. The correlations of year effects (r_Y) are estimated at the group level following Eq. 7 as described in Appendix 3.2 (Supporting Information) Materials and Methods for the entire period 1901–2003 (left panels) and for two consecutive periods (1901–1950 and 1951–2003; green and red dots, respectively) (right panels). The patterns are characterized as linear regressions of r_Y for each group (y-axis) on its corresponding latitude (x-axis). Significant linear trends along the latitudinal gradient are depicted as thick lines ($^{*}P < 0.05$; $^{***}P < 0.001$). Error bars denote standard errors.

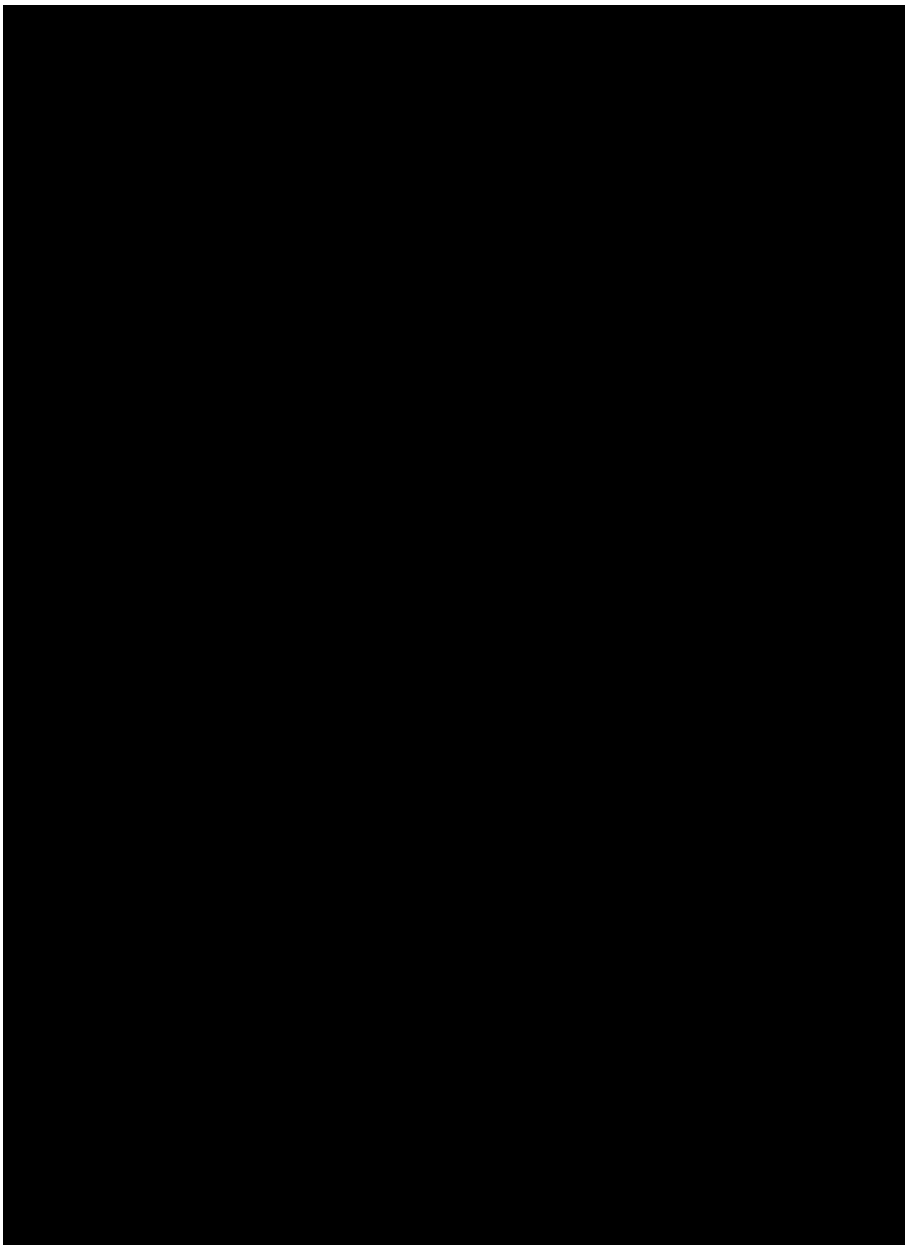

Figure S8. Patterns of the relationship between indexed tree-ring width (TRW_i) and carbon isotope discrimination ($\Delta^{13}C_i$) chronologies along climatic gradients across in Europe. The correlations of year effects (r_Y) are estimated at the group level following Eq. 7 as described in Appendix 3.2 (Supporting Information) **(a–c)** for the entire period of 1901–2003 and **(d–f)** for two consecutive periods (1901–1950 and 1951–2003). The patterns are characterized as linear regressions of r_Y for each group (y-axis) on its corresponding mean climate variable (x-axis) as follows: (*upper panels*) mean annual temperature (MAT); (*middle panels*) mean annual precipitation (MAP); (*lower panels*) mean annual potential evapotranspiration (PET). Significant linear trends along the climatic gradients are depicted as thick lines ($^{*}P < 0.05$; $^{**}P < 0.01$; $^{***}P < 0.001$). Error bars denote standard errors.

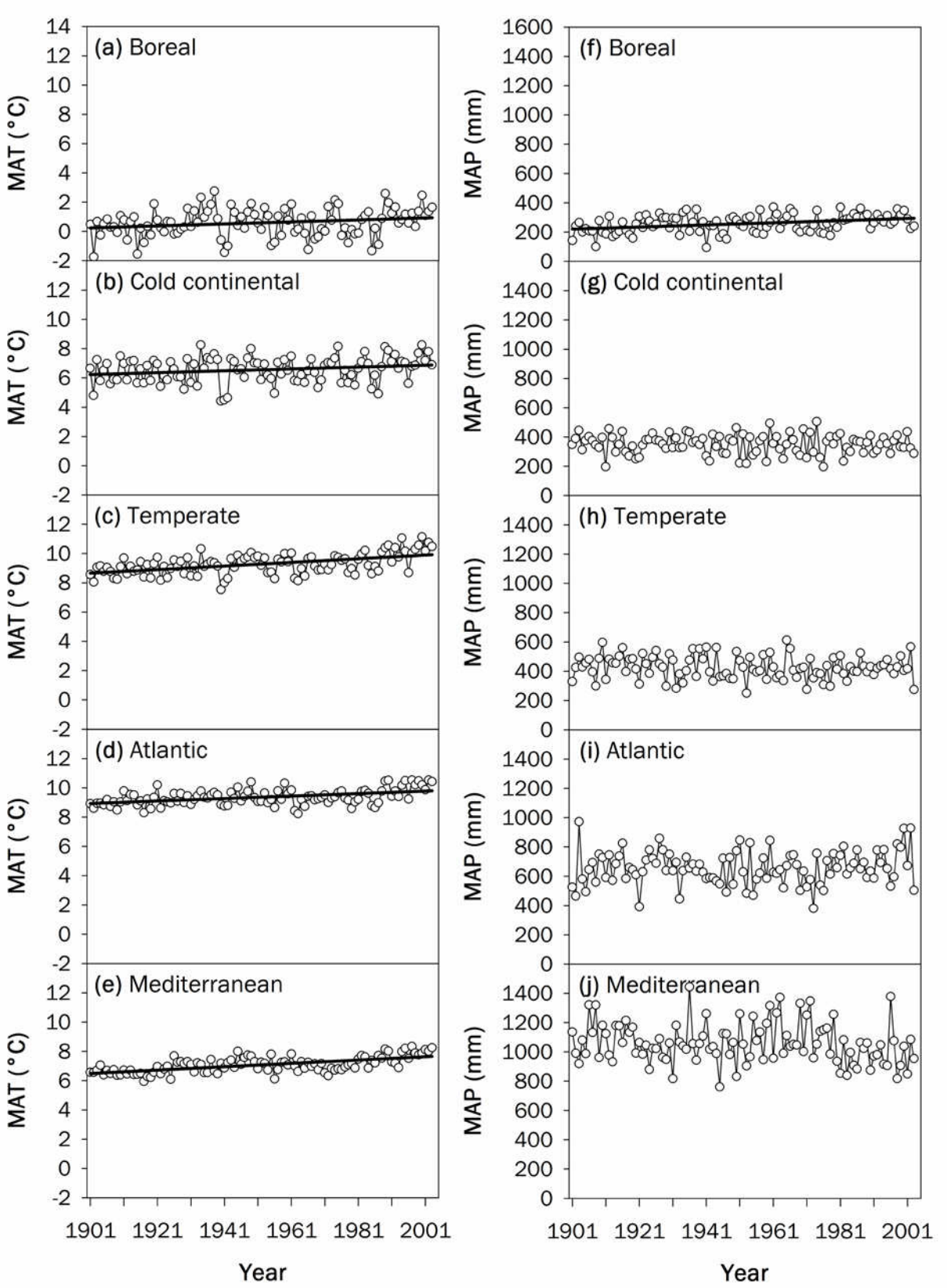

Figure S9. Trends in climate parameters at the group level: **(a-e)** mean annual temperature (MAT) and **(f-j)** mean annual precipitation (MAP). Significant linear trends along the climatic gradients are depicted as thick lines ($^{*}P < 0.05$).